

Structure of Coordination Complexes: The Synergy between NMR Spectroscopy and Computational Chemistry

Jeanet Conradie*

Department of Chemistry, University of the Free State, Bloemfontein, 9301, South Africa.

Received 6 September 2011, revised 8 November 2011, accepted 15 November 2011

Submitted by invitation to celebrate 2011 the 'International Year of Chemistry'

ABSTRACT

Illustrative examples of how NMR spectroscopy and computational chemistry data can be used in synergy to gain information on structure, coordination mode, bonding, symmetry and isomeric distribution of transition metal complexes, is presented. Isomer distribution and the most stable structures in a series of $\text{Ti}(\beta\text{-diketonato})_2\text{Cl}_2$ and $\text{Ti}(\beta\text{-diketonato})_2(\text{biphen})$ complexes as determined by density functional theory (DFT) methods and the application of the Boltzmann equation, are in agreement with crystal structures and variable temperature NMR results. Secondly, the DFT determined coordination mode of the 4-amino-3,5-bis(pyridine-2-yl)-1,2,4-triazole, (bpt-NH_2) which has the appropriate chemical geometry to behave as anionic or neutral bidentate chelating group to form a 5- or 6-membered complex, is shown to be in agreement with ^1H NMR shifts for $[\text{Rh}(\text{bpy})_2(\text{bpt-NH})]^{2+}$, $[\text{Rh}(\text{phen})_2(\text{bpt-NH})]^{2+}$, $[\text{Rh}(\text{bpt-NH})(\text{cod})]$ and $[\text{Ir}(\text{bpt-NH})(\text{cod})]$ ($\text{cod} = 1,5\text{-cyclooctadiene}$, $\text{phen} = 1,10\text{-phenanthroline}$, $\text{bpy} = 2,2'\text{-bipyridine}$). The oxidative addition of CH_3I to $[\text{Rh}(\beta\text{-diketonato})(\text{CO})(\text{PPh}_3)]$ complexes consist of three reaction steps and involves isomers of two different Rh^{III} -alkyl and two different Rh^{III} -acyl species. For this reaction experimental ^1H NMR techniques complement the stereochemistry of reaction intermediates and products as calculated by density functional theory. NMR properties, in agreement with computational results, proved to be useful to access the nature of the κ^3 to κ^2 distortion in coinage metal-ethylene complexes supported by tris(pyrazolyl)borates. The last example showed that NMR, X-ray crystal and computational results showed C_2 symmetry for a series of metal(II) complexes coordinated to a 16-membered pentaaza macrocycle.

KEYWORDS

DFT, computational, organometallic, NMR spectroscopy.

Table of Contents

1	Introduction	190
2	Computational Methods	191
3	Results and Discussion	191
3.1	Variable Temperature NMR Spectroscopy, Geometry and Isomer Distribution	191
3.2	Geometry and Coordination Mode	193
3.3	NMR Shifts and Structure	195
3.4	NOESY and Structure	196
3.5	Shielding and Structure	198
3.6	Bonding and Structure	199
3.7	Symmetry and Structure	200
	Acknowledgements	200
	References and Notes	200

1. Introduction

Computational chemistry is a branch of chemistry that uses principles of computer science to generate data which complements experimental data related to structures, properties and reactions of complexes. It uses the results of theoretical chemistry based primarily on the Schrödinger equation, to calculate the structures and electronic properties of molecules and solids. Any

computational method is just as good as its agreement with experiment. Good agreement with experimental results makes it possible to predict the properties and reactivity of related systems. Amongst more advanced techniques used in chemistry to characterize new complexes, like NMR spectroscopy, X-ray crystallography, elemental analysis and IR, only crystallography gives a complete picture of the structure of complexes. When no single crystals suitable for crystallography can be obtained,

* E-mail: conradj@ufs.ac.za

computational chemistry proved to be an obvious tool towards this end.

In the published literature there are several examples of the combined use of computational chemistry and experimental NMR spectroscopy towards understanding and solving stereochemistry of organic molecules. For example, solution NMR spectroscopy, single crystal X-ray diffractometry of related complexes and PM3 semi-empirical calculations (optimization of geometries and the calculations of heats of formation as a function of the dihedral angle) of the structure of N-formyl, N-acetyl-N-methyl and N-acetyl glycosylamines indicated an *anti* conformation around the glycosidic bond for these substances.¹ ¹⁹F NMR screening of fluorinated fragments in combination with crystal structure determination of related complex and computational analysis represents a sensitive and powerful approach for identifying fluorophilic hot-spots in proteins.² In medical chemistry a combined NMR spectroscopy and computational chemistry approach successfully determined the absolute stereochemistry of active enantiomers originating from human papillomavirus type-11 protein.³ A combined NMR and computational analysis of a series of 13 *cis/trans*-3,4-dihydro-2-alkoxy-4-(alkyl- or aryl-substituted)-2H,5Hpyrano[3,2-c][1]benzopyran-5-one derivatives allowed determination of the *cis/trans* configurations and conformational preferences. The conformational analysis of *cis* compounds, performed *via* NMR and computational studies, allowed the establishment of a preference for the conformer with both substituents in the pseudo-equatorial orientations. 2D NOESY spectra made assignment of *cis/trans* configuration possible with certainty.⁴

However, the combined use of computational chemistry and experimental NMR spectroscopy to elucidate the structure of complexes containing a transition metal is less known. The present overview does not attempt to give a full coverage of the available literature on the topic, but presents a number of illustrative examples that describe the synergy between experimental NMR⁵ spectroscopy and computational chemistry as to predict structure, with the focus on transition metal complexes.

2. Computational Methods

Density functional theory (DFT)^{6,7} is an important development in computational chemistry since it appears that new DFT methods may give equal or greater accuracy and efficiency for medium-sized or larger molecular systems at lower computational costs than *ab initio* methods.^{8,9} In DFT the energy is determined as a function of electron density. The different functionals used in density functional calculations on atoms and molecules are generally distinguished by the way that they treat the exchange (an attractive component of the electron–electron interaction energy) and correlation (energy difference between Hartree-Fock (HF) and experimental energy) components.

The simplest models, local density or spin density models are based on the assumption that the electron density is constant (or slowly varying) throughout space (Local Density Approximation, LDA or Local Spin Density Approximation, LSDA). Non-Local Density Functional methods or Gradient Corrected or Generalized Gradient Approximation (GGA) functionals involve both the values of the electron spin densities and its gradients (B or B88,¹⁰ LYP,¹¹ PW86,¹² PW91 or P91 or PW92,¹³ B95¹⁴). The so-called ‘pure’ density functionals (PW91, BP86, BLYP) require only the HF coulomb term while hybrid functionals make use of the HF exchange term.⁶ There are several hybrid functionals, such as the Adiabatic Connection

Model (ACM) and the Becke three parameter functional (B3), that define the exchange functional as a linear combination of Hartree-Fock, local, and gradient corrected exchange terms. This exchange functional is then combined with the local and/or gradient-corrected correlation functional. Examples of DFT hybrid functionals are B3LYP^{11,14,15} and B3PW91.^{15,16}

The DFT calculations reported in sections 3.1–3.5 were carried out with OLYP,^{15,17} PW91¹³ or B3LYP^{15,16} exchange-correlation functionals, all-electron STO-TZP basis sets, fine meshes for numerical integration of matrix elements, and suitably tight criteria for SCF and geometry optimization, all as implemented in the ADF 2009 program system.¹⁸ All complexes modelled were closed-shell (diamagnetic) species.

3. Results and Discussion

A couple of case studies¹⁹ are discussed to illustrate the synergy between experimental NMR spectroscopy and DFT computational chemistry to shed light on the structure of coordination complexes and intermediates. The first examples are Ti(β -diketonato)₂Cl₂,²⁰ Ti(β -diketonato)₂(biphen),²⁰ [Rh(bpy)₂(bpt-NH)]²⁺, [Rh(phen)₂(bpt-NH)]²⁺, [Rh(bpt-NH)(cod)]²⁺, Ir(bpt-NH)(cod),²¹ [Rh(β -diketonato)(P(OPh)₃)₂]²² and [Rh(β -diketonato)(CO)(PPh₃)₂]^{23,24} complexes (cod = 1,5-cyclooctadiene, phen = 1,10-phenanthroline, bpy = 2,2'-bipyridine, bpt-NH₂ = 4-amino-3,5-bis(pyridine-2-yl)-1,2,4-triazole, H₂biphen = 2,2'-biphenyldiol). Lastly examples of coinage metal-ethylene complexes supported by Tris(pyrazolyl)borates and metal(II) complexes coordinated to a 16-membered pentaaza macrocycle are also discussed.

3.1. Variable Temperature NMR Spectroscopy, Geometry and Isomer Distribution²⁰

Titanium(IV) complexes were widely studied for a variety of purposes, mainly serving as catalyst in different organic reactions^{25–30} as well as for antitumor activity.³¹ Two monomeric Ti(IV) complexes previously qualified for clinical trials on antitumour activity: Ti(ba)₂(OEt)₂ (budotitane, Hba = benzoylacetone)³² and TiCp₂Cl₂ (titanocene dichloride),³³ but second and third clinical phases were terminated mainly due to problems with the galenic formulation of compounds, i.e. the preparing and compounding of the medicines in order to optimize their absorption.³⁴ No information on the isomer distribution of budotitane in the galenic formulation used for tests of anticancer activity is available. It is therefore of importance to develop an understanding of the spatial arrangement of the monomeric Ti complex, and which of the five possible isomers of six-coordinate octahedrally configured Ti(ba)₂X₂ (X = OEt or Cl) complexes exhibit anticancer activity. We synthesized and characterized complexes related to the latter complexes, *viz.* dichlorobis(β -diketonato)titanium(IV) Ti(C₆H₅COCHCOR)₂Cl₂ and (2,2'-biphenyldiolato)bis(β -diketonato)titanium(IV) Ti(C₆H₅COCHCOR)₂(biphen) complexes with R = CH₃, C₆H₅ (Ph) and CF₃ and H₂biphen = 2,2'-biphenyldiol.³⁵ When R = C₆H₅ only one *cis* isomer is possible for both complexes. However, unsymmetrically substituted Ti(β -diketonato)₂Cl₂ and Ti(β -diketonato)₂(biphen) complexes can adopt three different *cis* orientations, see Fig. 1. Additionally, the Ti(β -diketonato)₂Cl₂ complexes can adopt two *trans* orientations. However, only Ti(β -diketonato)₂X₂ complexes with extremely bulky substituents such as iodide or *p*-dimethylaminophenoxy as hydrolyzable group X have the *trans* form.³² The isomeric configuration has been defined by three *cis* or *trans* prefixes which specify first the relative position of the Cl-ligands, then the relative orientation of the phenyl groups, and finally the relative orienta-

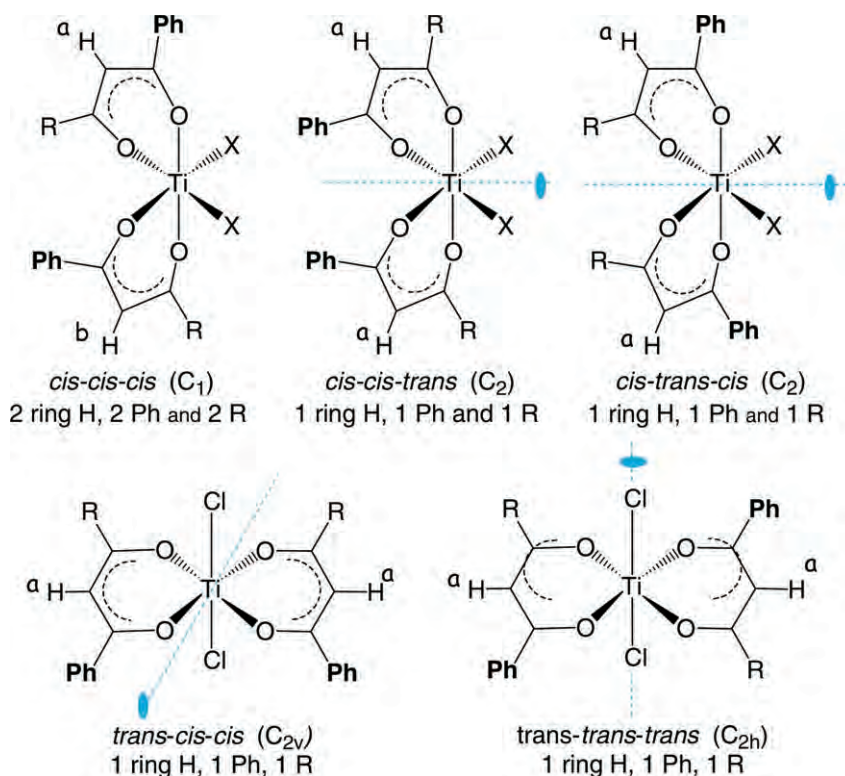


Figure 1 Stereochemistry of the isomers of asymmetrically substituted bis(β -diketonato) complexes of the type $\text{Ti}(\text{PhCOCHCOR})_2\text{Cl}_2$. The point group and the number of ^1H NMR signals are shown below each isomer.

tion of the R group on the β -diketonato ligand $\text{C}_6\text{H}_5\text{COCHCOR}$.

The crystal structures of $\text{Ti}(\text{C}_6\text{H}_5\text{COCHCOCH}_3)_2\text{Cl}_2$ ³⁴ and $\text{Ti}(\text{C}_6\text{H}_5\text{COCHCOCH}_3)_2(\text{biphen})$ ²⁰ are both known. Density functional theory (DFT) calculations were carried out on the five different isomers of $\text{Ti}(\text{C}_6\text{H}_5\text{COCHCOCH}_3)_2\text{Cl}_2$ and the three different $\text{Ti}(\text{C}_6\text{H}_5\text{COCHCOCH}_3)_2(\text{biphen})$ isomers. ADF calculated relative energies are given in Table 1.

Especially pleasing is the fact that the lowest energy (most stable) calculated isomer in both cases agrees with the isomer characterized by X-ray crystallography. Excellent agreement with the experimental structures is obtained as reflected by the RMSD values of 0.061 and 0.041 Å for $\text{Ti}(\text{C}_6\text{H}_5\text{COCHCOCH}_3)_2\text{Cl}_2$ and $\text{Ti}(\text{C}_6\text{H}_5\text{COCHCOCH}_3)_2(\text{biphen})$ respectively. The root-mean-square distances (RMSD) calculated for non-

hydrogen atoms for the best three-dimensional superposition of calculated structures on experimental structures give a qualitative measurement of the accuracy of the ground state geometry of the calculated structures. Structural data computed with this computational method for related compounds may therefore be presented with an equally high degree of accuracy. Density functional theory (DFT) calculations were thus also used in the study of the five different isomers of $\text{Ti}(\text{C}_6\text{H}_5\text{COCHCOCH}_3)_2\text{Cl}_2$ and the three different $\text{Ti}(\text{C}_6\text{H}_5\text{COCHCOCH}_3)_2(\text{biphen})$ isomers of which no crystal structures are known.³⁶ Relative energies are given in Table 1. DFT calculated relative energies of three *cis* isomers of each complex clearly highlight geometry preferences and also enable a population analysis of the isomers by application of the Boltzmann equation. DFT calculated geome-

Table 1 Observed and PW91/TZP calculated isomer distribution of $\text{Ti}(\text{PhCOCHCOR})_2\text{Cl}_2$ and $\text{Ti}(\text{PhCOCHCOR})_2(\text{biphen})$ complexes, R = CF_3 , CH_3 or Ph.

R	Isomer	$\text{Ti}(\text{PhCOCHCOR})_2\text{Cl}_2$			$\text{Ti}(\text{PhCOCHCOR})_2(\text{biphen})$		
		% Observed ^1H NMR	Relative energy/ kJ mol^{-1}	% Calc.	% Observed ^1H NMR	Relative energy/ kJ mol^{-1}	% Calc.
CH_3	<i>cis-cis-cis</i>	27.9	1.7	31.0	25.6	1.7	26.5
	<i>cis-trans-cis</i> (crystal structure)	54.7	0	61.7	49.2	0	43.7
	<i>cis-cis-trans</i>	17.4	5.5	6.7	25.2	1.4	29.8
	<i>trans-trans-trans</i>	0.0	12.0	0.5	-	-	-
	<i>trans-cis-cis</i>	0.0	15.2	0.1	-	-	-
Ph	<i>cis-cis-cis</i>	100.0	0	97.1	100.0	0	100.0
	<i>trans-trans-trans</i>	0.0	8.7	2.9	-	-	-
CF_3	<i>cis-cis-cis</i>	21.5	0.2	39.5	17.1	2.9	19.5
	<i>cis-trans-cis</i>	40.6	0	41.9	62.4	0	62.2
	<i>cis-cis-trans</i>	38.0	2.0	18.4	20.6	3.0	18.3
	<i>trans-trans-trans</i>	0.0	13.8	0.2	-	-	-
	<i>trans-cis-cis</i>	0.0	21.3	0.0	-	-	-

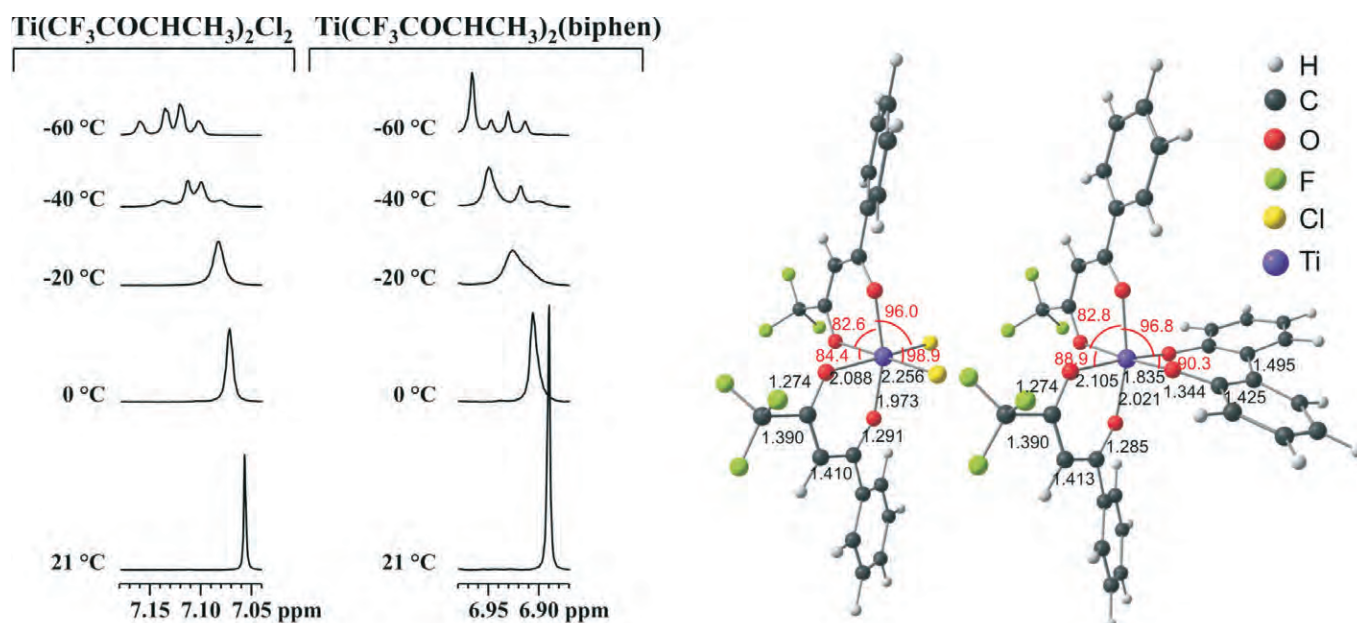


Figure 2 Left: variable temperature ¹H NMR spectra of the indicated complexes showing methine (*ca.* 7 ppm) resonances. Right: DFT calculated geometry of the major isomer of Ti(C₆H₅COCHCOCF₃)₂Cl₂ and Ti(C₆H₅COCHCOCF₃)₂(biphen).

tries of the major isomers of Ti(C₆H₅COCHCOCF₃)₂Cl₂ and Ti(C₆H₅COCHCOCF₃)₂(biphen) are shown in Fig. 2.

The stereochemistry of Ti(C₆H₅COCHCOCF₃)₂Cl₂ and Ti(C₆H₅COCHCOCF₃)₂(biphen), however, can also partly be inferred from NMR spectra. The *cis-cis-cis* isomer with no symmetry (point group C₁) may give rise to two phenyl and two ring proton resonances. The other four isomers, *cis-trans-cis* (point group C₂), *cis-cis-trans* (C₂), *trans-cis-cis* (C_{2v}) and *trans-trans-trans* (C_{2h}) all possess at least a twofold axis and should give a single resonance for each type of group. At room temperature (294 K) only one single set of ¹H NMR signals was observed for Ti(C₆H₅COCHCOCF₃)₂Cl₂ and Ti(C₆H₅COCHCOCF₃)₂(biphen). The resonance signal of the methine H is sharp due to rapid isomerization (relative to the NMR time scale) which exchanges groups between non equivalent environments. When lowering temperature, these signals broaden and split up into four signals, see Fig. 2. When the temperature is increased the four signals that were observed at -60 °C collapse into a singlet as a result of rapid isomerization at room temperature. The four distinguishable signals of three different intensities at -60 °C are consistent with the existence of three *cis* isomers in CDCl₃ solution. The two spectral lines of equal intensity are assigned to the *cis-cis-cis* isomer. The experimentally observed *cis-trans-cis* and *cis-cis-trans* populations are assigned according to the calculated isomer distribution. A generally good agreement is obtained between experimentally observed isomer distribution and calculated values, see Table 1. This example thus highlight the synergy between NMR spectroscopy and computational chemistry in order to get a better understanding of the geometry and isomer distribution in Ti(C₆H₅COCHCOCR)₂Cl₂ and Ti(C₆H₅COCHCOCR)₂(biphen) complexes.

3.2. Geometry and Coordination Mode²¹

Over 60 per cent of acetic acid made for use in the chemical industry is made by methanol carbonylation using rhodium and iridium as catalysts.³⁷ The first major process in the carbonylation of methanol was developed by Monsanto in the 1970s using [Rh(I)₂(CO)₂]⁻ as catalyst.³⁸ In 1996 BP Chemicals announced a new advanced technology, called the Cativa process, which

Table 2 NH ¹H NMR signal shifts of complexes and ligands in acetone-d₆, DMSO-d₆ and CDCl₃^a

Compound	Ring-size	δ _i (H) of NH/ppm		
		Acetone-D	DMSO-d	CDCl ₃
bpt-NH ₂	–	8.76	7.82	8.55
[Rh(bpt-NH ₂)(cod)] ⁺	5	8.51		
[Rh(bpy) ₂ (bpt-NH ₂)] ³⁺	5		7.66	
[Rh(bpy) ₂ (bpt-NH)] ²⁺	6		9.16	
[Rh(phen) ₂ (bpt-NH)] ²⁺	6		9.11	
[Rh(bpt-NH)(cod)]	6			9.16
[Ir(bpt-NH)(cod)]	6			10.92

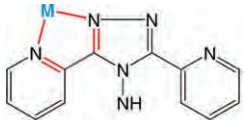
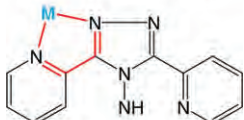
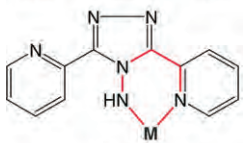
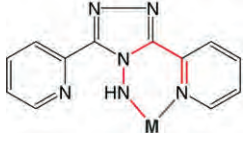
^a Data from references 21, 52 and 53.

replaced rhodium with iridium catalysts, in conjunction with novel promoters such as rhenium, ruthenium and osmium. Benefits achieved with the change in catalyst include cheaper iridium prices, a faster and more effective process, less catalyst required, larger turnover numbers and less side products.³⁹ Research has shown that the actual catalytic cycles of the Monsanto and Cativa⁴⁰ processes consist of a series of reactions including oxidative addition, 1,1-insertion or CO insertion, CO association and reductive elimination.^{2,3,4} Oxidative addition and CO insertion reactions in rhodium(I) and iridium(I) complexes were studied in detail in our laboratories,^{44–48} and by a large number of researchers.^{49–51} It involved structural and mechanistic studies by manipulation of e.g. the nucleophilicity of the metal center using different mono and bidentate ligands, or changing the steric bulk within the complex to change the rate of the different key reactions in the process.

One such ligand is 4-amino-3,5-bis(pyridine-2-yl)-1,2,4-triazole, (bpt-NH₂), which has the appropriate chemical geometry to behave as an anionic or neutral bidentate chelating group to form a 5-membered M'(bpt-NH)(LL), or 5-membered M'(bpt-NH₂)(LL)⁺, or 6-membered M'(bpt-NH)(LL) complex, LL = neutral ligand (bidentate or two monodentate).²¹

The difference between these two coordination modes is deduced from a ¹H NMR perspective. Formation of the

Table 3 DFT (B3LYP/TZP) molecular energies (kJ/mol) of the possible coordination modes and stereo isomers of $[M(\text{bpt-NH})(\text{cod})]$, $M = \text{Ir}$ or Rh , $[\text{Rh}(\text{phen})_2(\text{bpt-NH})]^{2+}$ and $[\text{Rh}(\text{bpy})_2(\text{bpt-NH})]^{2+}$ relative to the lowest energy isomer in each case.

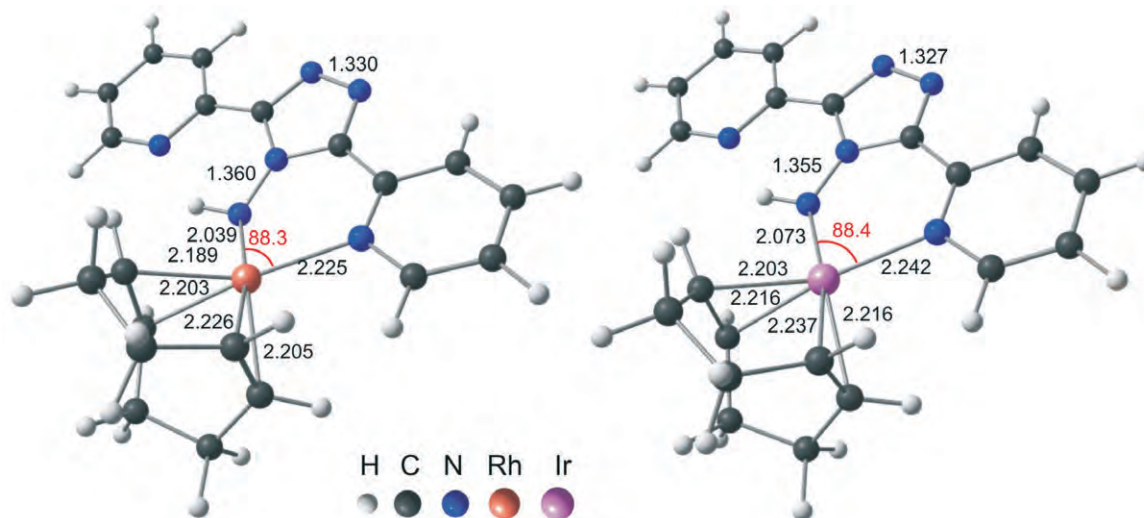
Geometry	5- or 6-membered ring	Energy/kJmol ⁻¹			
		$[\text{Ir}(\text{bpt-NH})(\text{cod})]$	$[\text{Rh}(\text{bpt-NH})(\text{cod})]$	$[\text{Rh}(\text{bpy})_2(\text{bpt-NH})]^{2+ \text{ a}}$	$[\text{Rh}(\text{phen})_2(\text{bpt-NH})]^{2+ \text{ a}}$
	5	50.1	37.0	56.6	75.1
	5	23.8	19.7	34.8	54.3
	6	72.3	41.1	68.5	^b
	6	0.0	0.0	0.0	0.0

^a Calculations of the present study.^b This geometry spontaneously optimized to the lowest energy geometry.

6-membered ring structure should give rise to a significant downfield shift of the singlet associated with the amide moiety with respect to the free ligand, see Table 2 for a summary. The singlet associated with the NH moiety was found at 10.92 and 9.16 ppm for $[\text{Ir}(\text{bpt-NH})(\text{cod})]$ and $[\text{Rh}(\text{bpt-NH})(\text{cod})]$ respectively, whereas that of the free ligand was observed at 8.55 ppm in CDCl_3 ($\text{cod} = 1,5\text{-cyclooctadiene}$). This result indicates a 6-membered coordination mode. A similar downfield shift has been observed for the singlet associated with the NH moiety of 6-membered $[\text{Rh}(\text{phen})_2(\text{bpt-NH})]^{2+}$ and 6-membered $[\text{Rh}(\text{bpy})_2(\text{bpt-NH})]^{2+}$ (9.11 and 9.16 ppm respectively in $d_6\text{-DMSO}$) relative to that of the free ligand at 7.82 ppm in $d_6\text{-DMSO}$ ($\text{phen} = 1,10\text{-phenanthroline}$, $\text{bpy} = 2,2'\text{-bipyridine}$).⁵² However, the singlet associated with the NH moiety of the

5-membered $[\text{Rh}(\text{bpt-NH}_2)(\text{cod})]^+$ and $[\text{Rh}(\text{bpy})_2(\text{bpt-NH}_2)]^{3+}$ complexes were found at 8.51 ($d_6\text{-acetone}$)⁵³ and 7.66 ppm ($d_6\text{-DMSO}$) respectively which is comparable to that of the free ligand (8.76 ppm in $d_6\text{-acetone}$ ⁵³ and 7.82 ppm in $d_6\text{-DMSO}$).⁵²

In further support of the coordination mode of $[\text{Ir}(\text{bpt-NH})(\text{cod})]$ and $[\text{Rh}(\text{bpt-NH})(\text{cod})]$ density functional theory calculations on the possible isomers of the two coordination modes of the bpt-NH ligand to rhodium(I) and iridium(I) in $[\text{Ir}(\text{bpt-NH})(\text{cod})]$ and $[\text{Rh}(\text{bpt-NH})(\text{cod})]$ were performed. In agreement with NMR spectroscopic data,²¹ calculations showed the 6-membered ring complexes with the nitrogen of the uncoordinated pyridine ring rotated in the same direction as the amine moiety, being more stable by 23.8–72.3 kJ mol⁻¹ (see Table 3). The minimum energy optimized structures of $[\text{Ir}(\text{bpt-NH})(\text{cod})]$ and

**Figure 3** DFT calculated geometry of $[\text{Rh}(\text{bpt-NH})(\text{cod})]$ (left) and $[\text{Ir}(\text{bpt-NH})(\text{cod})]$ (right).

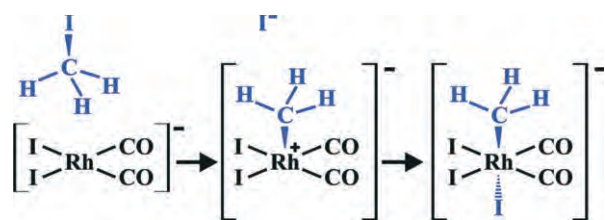


Figure 4 S_N2 mechanism for the oxidative addition of methyl iodide to the Monsanto catalyst, cis -[Rh(CO) $_2$ I] $_2$ leading to a $trans$ oxidative addition product.

[Rh(bpt-NH)(cod)] are presented in Fig. 3, with selected bond lengths and angles shown. DFT calculations of this study on the possible coordination modes of [Rh(bpy) $_2$ (bpt-NH)] $^{2+}$ and [Rh(phen) $_2$ (bpt-NH)] $^{2+}$ are also shown, and are in agreement with experiment, with 6-coordinated [Rh(bpy) $_2$ (bpt-NH)] $^{2+}$ at lowest energy.

3.3. NMR Shifts and Structure 22

The oxidative addition reaction of methyl iodide to cis -[Rh(CO) $_2$ I] $_2$ $^{-40,42,54}$ is the first catalytic step in the methanol carbonylation process with the Monsanto catalyst. $^{55-61}$ It is widely accepted that oxidative addition of methyl iodide to square planar rhodium(I) complexes occurs *via* a two-step mechanism involving nucleophilic attack by the metal on the methyl carbon to displace iodide during formation of the metal-carbon bond. This reaction is presumed to proceed with inversion of configuration at the carbon and coordination of iodide to the five-coordinated intermediate to give a six-coordinated alkyl complex, see Fig. 4. 55,61,62 The mechanism involves *trans* addition of methyl iodide to the square planar rhodium(I) complex. The observation of *cis* products has sometimes been taken as evidence for an alternative concerted three-centre mechanism leading to retention of configuration at the carbon. $^{63-65}$ Since understanding of the mechanism of activity of a catalyst requires an understanding of its structure in all reaction steps, an example of how both 1 H NMR spectroscopy and computational chemistry results indicate *trans* addition of methyl iodide to β -diketonatobis(triphenylphosphite)-rhodium(I) complexes, is presented here. 22,66

The stereochemistry of the product of oxidative addition of methyl iodide to [Rh(acac)(P(OPh) $_3$) $_2$] (Hacac = acetylacetonate = CH $_3$ COCH $_2$ COCH $_3$), the rhodium(III)-alkyl complex [Rh(acac)(P(OPh) $_3$) $_2$ (CH $_3$)(I)] was determined from 1 H NMR spectra $^{67-69}$



Figure 5 Four possible [Rh(acac)(P(OPh) $_3$) $_2$ (CH $_3$)(I)] reaction products of the [Rh(acac)(P(OPh) $_3$) $_2$] + CH $_3$ I reaction with PW91/TZP/methanol calculated energies (ΔE_{TBE}) listed below each alkyl. Alkyl-A (lowest energy) result from *trans* addition, alkyl-B, alkyl-C and alkyl-D represent the various *cis* isomers. Energies of reactants are taken as zero.

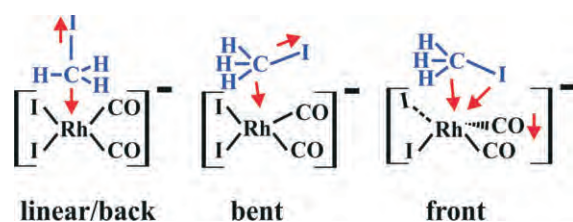


Figure 6 Schematic illustration of linear, bent and front transition states for the nucleophilic attack of square planar rhodium(I) on methyl iodide. The movement of applicable atoms in the transition state is indicated by red arrows. The Monsanto catalyst [Rh(CO) $_2$ I] $_2$ $^{-}$ is used in this figure as example of the square planar rhodium(I) complex.

The 1 H NMR spectrum of [Rh(acac)(P(OPh) $_3$) $_2$ (CH $_3$)(I)] shows two methyl signals. The singlet at 1.43 ppm (acetone- d_6) for the two CH $_3$ side groups of the bidentate ligand acac, suggests that these two CH $_3$ groups of the β -diketonato ligand are magnetically equivalent. The methyl signal of the addend (CH $_3$ of methyl iodide) appears as a double doublet due to its coupling with Rh (spin = $1/2$) and P (spin = $1/2$). This indicates that the CH $_3$ is directly bonded to Rh as in an alkyl complex. Based on this 1 H NMR spectroscopic data, the structure of [Rh(acac)(P(OPh) $_3$) $_2$ (CH $_3$)(I)] is thus proposed to adopt an octahedral geometry in which the acac ligand and the two triphenylphosphite groups are located in an equatorial plane with the methyl and iodide ligands in the axial positions. No solid state X-ray crystal structure has been solved for the product. 36 Crystal data in support of the proposed *trans*-[Rh(acac)(P(OPh) $_3$) $_2$ (CH $_3$)(I)] structure, is the structure of *trans*-[Rh(N-benzoyl-N-phenylhydroxyamino)(P(OPh) $_3$) $_2$ (CH $_3$)(I)] 70 and *trans*-[Rh(trifluoroacetylacetonato)(P(OPh) $_3$) $_2$ (I)] 71 .

In further support of the geometry of [Rh(acac)(P(OPh) $_3$) $_2$ (CH $_3$)(I)] density functional theory calculations were done on four possible rhodium(III) alkyl isomers: (Alkyl-A) if *trans* addition occurs and three possible isomers (Alkyl-B, Alkyl-C and Alkyl-D) if *cis* addition occurs. 22 The isomers and their ADF optimized relative electronic energies are displayed in Fig. 5. These energies, in agreement with 1 H NMR spectroscopic data, indicate the *trans* alkyl product A as being the most stable product of oxidative addition of methyl iodide to [Rh(acac)(P(OPh) $_3$) $_2$].

Figure 6 displays the three types of TS structures that have been reported for the oxidative addition of methyl iodide to square planar rhodium(I) complexes (especially the Monsanto catalyst [Rh(CO) $_2$ I] $_2$ $^{-}$). 55,72 Two transition states lead to *trans* addition ('linear' and 'bent') and one to *cis* addition ('front'). The linear TS structure corresponds to a S_N2 mechanism, characterized by a linear Rh-C $_{CH_3}$ -I arrangement and by a Rh-C $_{CH_3}$ -H angle close to 90°. The methyl hydrogen atoms are located in the equatorial plane of the five-coordinated carbon atom, resulting in a trigonal bipyramidal arrangement. The bent and front TS structures correspond to a side-on approach of the C $_{CH_3}$ -I bond to the rhodium atom. The bent transition state structure leads to the same intermediate product as the linear transition state structure—a cationic five-coordinated rhodium complex and a free iodide ion. 55 Both the mechanisms of the linear and the bent transition state structures are therefore described as S_N2 processes. The front TS structure corresponds to a concerted three-centre oxidative addition, in which the Rh-I and Rh-C $_{CH_3}$ bonds form simultaneously as the I-C $_{CH_3}$ bond breaks, resulting in the *cis* addition of the methyl iodide. The linear transition state for the [Rh(acac)(P(OPh) $_3$) $_2$] + CH $_3$ I reaction, 22 as was also found for the Monsanto catalyst, 72 is favoured by a large margin of energy

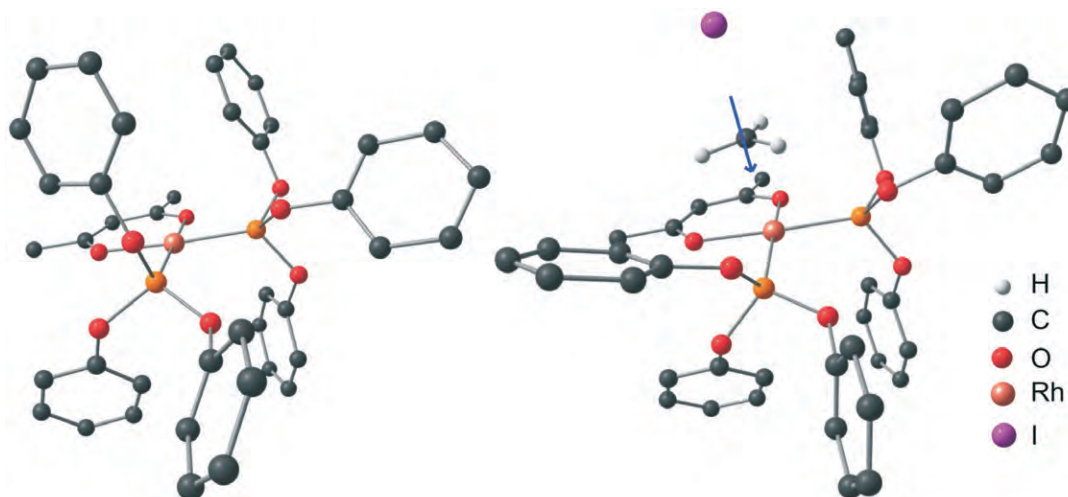


Figure 7 PW91/TZP/methanol optimized structure of the rhodium(I) reactant (left) and the TS (right) of the $[\text{Rh}(\text{acac})(\text{P}(\text{OPh})_2)] + \text{CH}_3\text{I}$ reaction. H atoms are removed for clarity (except for the methyl group of CH_3I). The square pyramidal TS, involving attack of rhodium on the CH_3^+ group with displacement vector (blue arrow), indicating movement of the CH_3^+ group at negative frequency (-258.6 cm^{-1}). In the reactant $[\text{Rh}(\text{acac})(\text{P}(\text{OPh})_2)]$, the large OPh groups are bent backwards so that the Ph groups are arranged above, below and in the plane (formed by the acac-ligand, the rhodium atom and the two phosphorus atoms). As the CH_3I group approaches the reactant, the 'arms' of the OPh groups above the plane gradually open up to accept the incoming CH_3I group to proceed through the TS.

($> 90 \text{ kJ mol}^{-1}$) with activation barrier (ΔE_a) of 30 kJ mol^{-1} . The linear transition state leads to the *trans* alkyl product A of oxidative addition of methyl iodide to $[\text{Rh}(\text{acac})(\text{P}(\text{OPh})_2)]$, in agreement with ^1H NMR spectroscopy data.⁶⁸ The DFT optimized $[\text{Rh}(\text{acac})(\text{P}(\text{OPh})_2)]$ and the linear TS are visualized in Fig. 7.

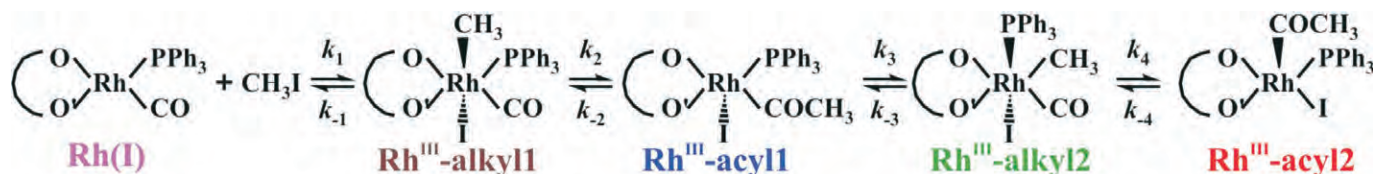
3.4. NOESY and Structure²³

The reaction between methyl iodide and $[\text{Rh}(\text{acac})(\text{CO})(\text{PPh}_3)]$ (Hacac = acetylacetonate) is another Monsanto analogue. The main difference between the Monsanto process and this reaction^{73–78} is that no carbonyl addition and reductive elimination steps occur as is the case with the Monsanto process itself. While the stereochemistry of the product of oxidative addition of methyl iodide to $[\text{Rh}(\text{acac})(\text{P}(\text{OPh})_2)]$ could be determined from one dimensional ^1H NMR spectroscopy, it is not possible for the $[\text{Rh}^{\text{I}}(\text{acac})(\text{CO})(\text{PPh}_3)] + \text{CH}_3\text{I}$ product, since the two CH_3 side groups on acac are not magnetically equivalent. Since the $[\text{Rh}^{\text{I}}(\text{acac})(\text{CO})(\text{PPh}_3)]$ contains a CO group, CO insertion in the CH_3 addend group occurs according to Scheme 1.

The notations 'Rh^{III}-alkyl1' and 'Rh^{III}-acyl1' in Scheme 1 respectively refer to the first alkylated $[\text{Rh}^{\text{III}}(\text{acac})(\text{CH}_3)(\text{CO})(\text{PPh}_3)(\text{I})]$ and the first acylated $[\text{Rh}^{\text{III}}(\text{acac})(\text{COCH}_3)(\text{PPh}_3)(\text{I})]$ complexes that are formed. When the last number in the notation changes to '2', as in 'Rh^{III}-alkyl2', it shows that after the first alkylated complex had been formed, it converted to a second different, but more stable alkylated structural isomer. The DFT calculated lowest energy of the $[\text{Rh}^{\text{III}}(\text{acac})(\text{CH}_3)(\text{CO})(\text{PPh}_3)(\text{I})]$ -alkyl product will thus not necessarily be the first product of oxidative addition. Also, due to the equilibrium between the different

reaction products, it was not yet possible to isolate the different reaction products. Representative ^1H NMR spectra of a sample recorded *in situ* 10' minutes after the reaction $[\text{Rh}(\text{acac})(\text{CO})(\text{PPh}_3)] + \text{CH}_3\text{I}$ has been initiated, are given in Fig. 8 (the region of phenyl protons of the triphenylphosphine ligand (PPh_3) is excluded). The signals in the ^1H NMR spectra of the reaction were assigned to the applicable Rh(III) complexes by monitoring the relative decrease and increase of the peaks as the reaction proceeds, and by comparing it with data obtained by Varshavsky *et al.*⁷⁵ and other related reactions.

^1H Nuclear Overhauser Effect Spectroscopy (NOESY)^{82–84} in this case provides valuable information on the stereochemistry of reaction products, although no crystals suitable for X-ray analysis of the Rh(III) reaction products have been obtained.³⁶ NOE differs from spin coupling in that NOE is observed through space, not through bonds. Thus, all atoms in proximity to each other give NOE's, whereas spin coupling is observed only when the atoms are bonded to the same or neighbouring atoms. A one dimensional (1D) ^1H NOESY was recorded *in situ* during this reaction, to establish the relative positions of the ligands in Rh^{III}-alkyl1, see Fig. 9.²³ Irradiation of the Rh- CH_3 resonance of Rh^{III}-alkyl1 (at *ca* 1.4 ppm) gave an NOE showing the PPh_3 group, the methine proton and the CH_3 side groups of the acac ligand (Fig. 9). The NOE with the methine proton rules out the possibility of the CH_3 group being in the square plane formed by the β -diketonato ligand and the other two groups bonded to the rhodium centre. The CH_3 group, bonded to the rhodium centre of Rh^{III}-alkyl1, is thus in the axial position, with the PPh_3 group adjacent to the CH_3 group. The PPh_3 group is



Scheme 1

Proposed reaction scheme of the reaction of methyl iodide with $[\text{Rh}(\text{acac})(\text{CO})(\text{PPh}_3)]$ where OO' = acac. Stereochemistry is assigned according to IR, NMR spectroscopy and computational chemistry results.²³ This scheme was found to be applicable to all $[\text{Rh}(\beta\text{-diketonato})(\text{CO})(\text{PPh}_3)] + \text{CH}_3\text{I}$ reactions.^{77,80}

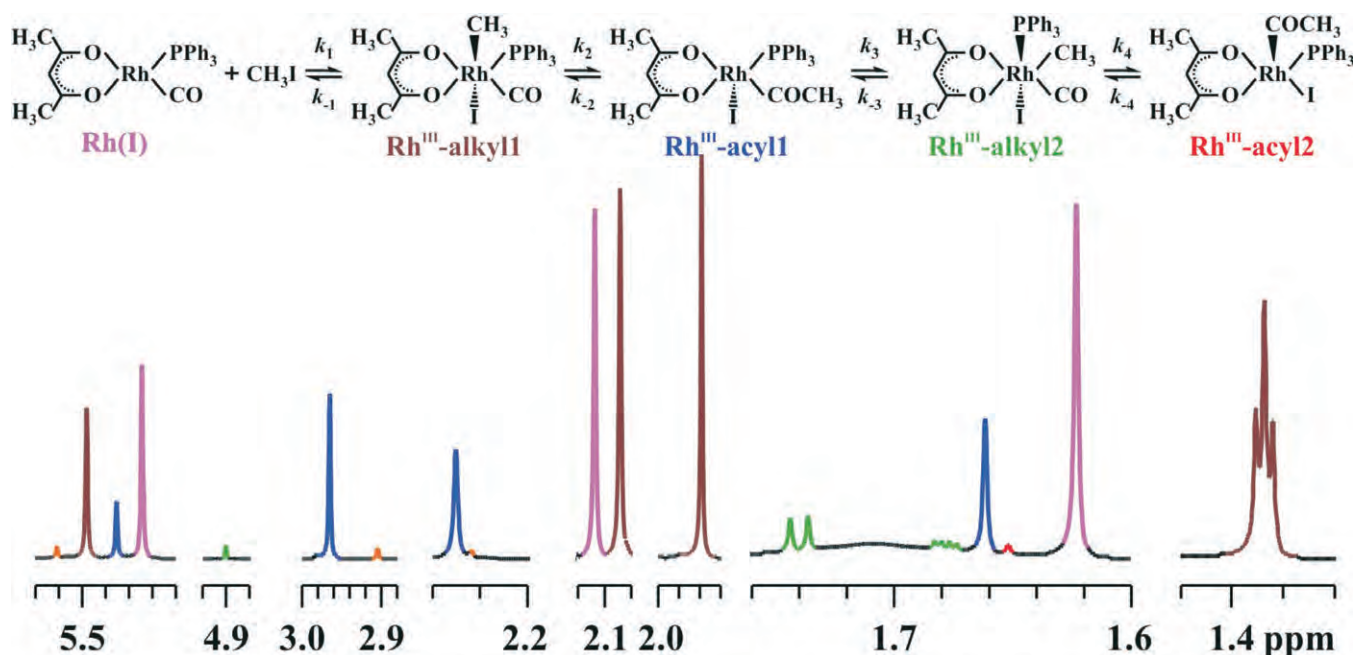


Figure 8 ^1H NMR spectra of the reaction of methyl iodide with $[\text{Rh}(\text{acac})(\text{CO})(\text{PPh}_3)]$ recorded at 10 minutes after the reaction had been initiated. Peaks are colour coded according to $\text{Rh}(\text{I})$ and $\text{Rh}(\text{III})$ complexes in the proposed reaction scheme shown at the top.²³

thus in the square plane surrounding rhodium. From the 1D ^1H NOESY spectrum it is not possible to establish whether the CO group or the iodide is adjacent to the CH_3 group, since these groups do not contain any protons. However, all crystal structures of $[\text{Rh}^{\text{III}}(\text{L},\text{L}'\text{-BID})(\text{CH}_3)(\text{CO})(\text{PPh}_3)(\text{I})]$ complexes (L,L'-BID = a mono-charged bidentate ligand with donor atoms L and L') to date have the CO group in the square plane formed by the β -diketonato ligand and the other two groups bonded to the rhodium centre and the iodide in apical position.^{36,78,85–88}

These results are thus consistent with *trans* $[\text{Rh}^{\text{III}}(\text{acac})(\text{CH}_3)(\text{CO})(\text{PPh}_3)(\text{I})]$ -alkyl1, in agreement with the proposed stereochemistry of the Rh^{III} -alkyl1 complex in Scheme 1.

In further support of the geometry of $[\text{Rh}^{\text{III}}(\text{acac})(\text{CO})(\text{PPh}_3)(\text{CH}_3)(\text{I})]$ -alkyl1 density functional theory calculations were done to determine the transition state and first product of oxidative addition.²³ DFT calculated activation energies (ΔE_a) of the three possible transition states for the oxidative addition of methyl iodide to square planar $\text{Rh}(\text{I})$ complexes (Fig. 6) were

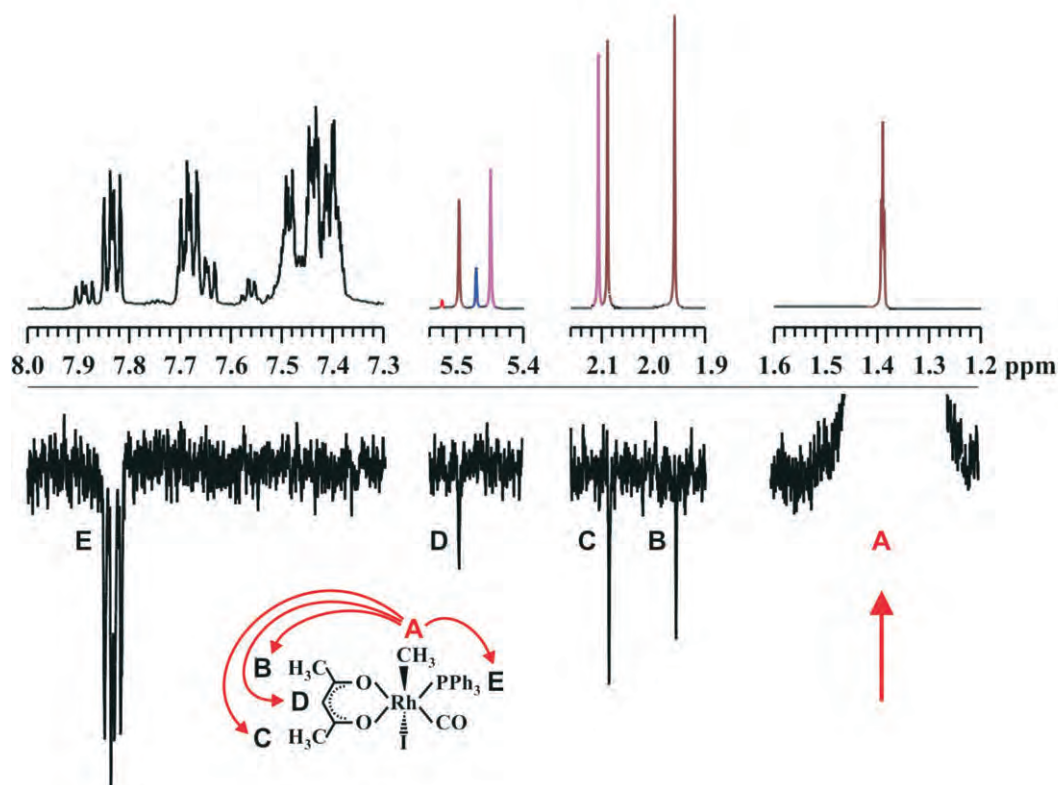


Figure 9 ^1H NMR (top) and 1D ^1H NOESY (bottom) of $[\text{Rh}^{\text{III}}(\text{acac})(\text{CO})(\text{PPh}_3)(\text{CH}_3)(\text{I})]$ -alkyl1, pulsating on the Rh- CH_3 resonance at ca. 1.4 ppm. NOE is as illustrated.²³

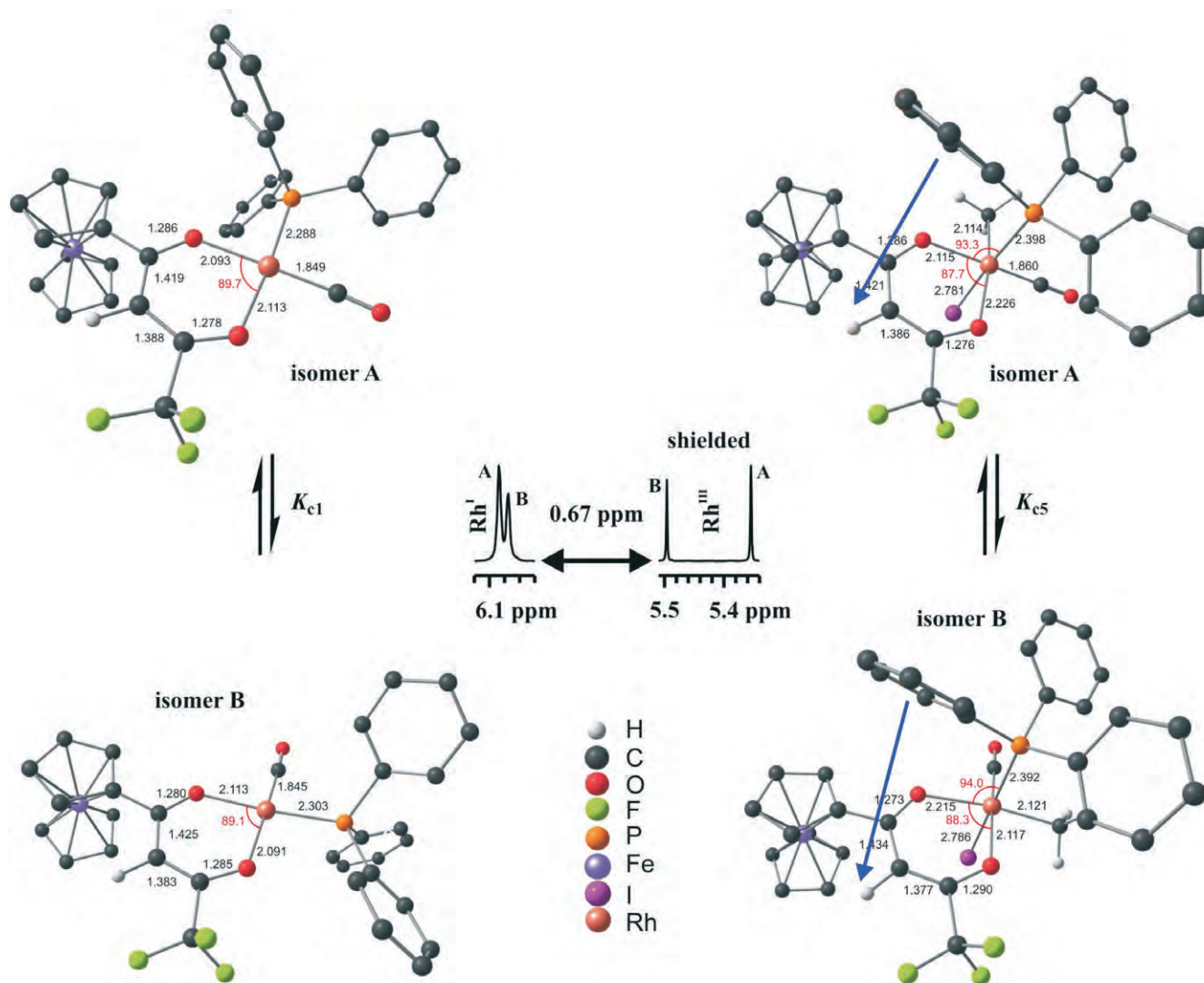


Figure 10 PW91/TZP optimized structures of $[\text{Rh}(\text{fctfa})(\text{CO})(\text{PPh}_3)]$ (left) and of $[\text{Rh}(\text{fctfa})(\text{CH}_3)(\text{CO})(\text{PPh}_3)(\text{I})\text{-alkyl}2]$ (right), illustrating the shielding effect of the phenyl ring on the methyl proton in alkyl2 resulting in an upfield shift. Two isomers of each are observed. Isomers A were also characterized by X-ray crystal structures. Middle: The methine region of the ^1H NMR spectrum of $[\text{Rh}(\text{fctfa})(\text{CO})(\text{PPh}_3)]$ and $[\text{Rh}(\text{fctfa})(\text{CH}_3)(\text{CO})(\text{PPh}_3)(\text{I})\text{-alkyl}2]$.

24 kJ mol^{-1} (linear/back), 141 kJ mol^{-1} (bent) and 138 kJ mol^{-1} (front). The linear/back transition state thus has the lowest activation barrier ($\Delta E_a = 24 \text{ kJ mol}^{-1}$). The linear transition state leads to a *trans* $[\text{Rh}^{\text{III}}(\text{acac})(\text{CO})(\text{PPh}_3)(\text{CH}_3)(\text{I})\text{-alkyl}1]$ product of oxidative addition of methyl iodide to $[\text{Rh}(\text{acac})(\text{CO})(\text{PPh}_3)]$, in agreement with the ^1H NOESY NMR data. (The reader is referred to ref. 23 for a comprehensive discussion on NMR spectroscopy and computational chemistry results of the $[\text{Rh}(\text{acac})(\text{CO})(\text{PPh}_3)] + \text{CH}_3\text{I}$ reaction.)

3.5. Shielding and Structure²⁴

The reaction between $[\text{Rh}^{\text{I}}(\text{fctfa})(\text{CO})(\text{PPh}_3)]$ and methyl iodide ($\text{Hfctfa} = 1\text{-ferrocenyl-4,4,4-trifluorobutane-1,3-dione}$) also proceed according to Scheme 1. For this reaction, both the $[\text{Rh}(\text{fctfa})(\text{CO})(\text{PPh}_3)]$ reactant⁸⁹ and the $[\text{Rh}^{\text{III}}(\text{fctfa})(\text{CO})(\text{PPh}_3)(\text{CH}_3)(\text{I})\text{-alkyl}2]$ ⁷⁸ product were stable enough to be isolated from the reaction mixture and to be characterized by X-ray crystallography. In the crystal structure of $[\text{Rh}(\text{fctfa})(\text{CH}_3)(\text{CO})(\text{PPh}_3)(\text{I})\text{-alkyl}2]$ the PPh_3 group and iodide are above and below the square plane formed by the two oxygens of the β -diketonato ligand and the other two groups bonded to the rhodium centre, see Fig. 1 top right.^{24,78}

Information about the stereochemistry of $[\text{Rh}(\text{fctfa})(\text{CH}_3)(\text{CO})(\text{PPh}_3)(\text{I})\text{-alkyl}2]$ can also be inferred from ^1H NMR spectroscopy. Due to the unsymmetrical β -diketonato ligand, two structural isomers for rhodium(I) as well as for each rhodium(III) reaction intermediate (according to Scheme 1) are observed by NMR spectroscopy.⁷⁸ In CDCl_3 at 25°C , the signals of the methine proton of the β -diketonato ligand of the $[\text{Rh}(\text{fctfa})(\text{CO})(\text{PPh}_3)]$ isomers are at 6.08 and 6.09 ppm (Fig. 10),⁷⁸ while the signals of the methine proton of the β -diketonato ligand of the different $[\text{Rh}(\text{fctfa})(\text{CH}_3)(\text{CO})(\text{PPh}_3)(\text{I})\text{-alkyl}2]$ isomers are presented as singlets at 5.50 and 5.35 ppm.

The positioning of the PPh_3 group above (or below) the plane as in $\text{Rh-alkyl}2$, implies that as the PPh_3 group rotates, a Ph group will be rotating directly above the methine H of the β -diketonato ligand (Fig. 10 right). The ring current inside the phenyl ring shields the methine H directly below to higher field.⁹⁰ Thus, the observed shift of the methine proton of the β -diketonato ligand from ~ 6.0 ppm for Rh^{I} to higher field at ~ 5.4 ppm for $\text{Rh}^{\text{III}}\text{-alkyl}2$ is consistent with the PPh_3 group being positioned above (or below) the plane. (By the same reasoning, it is thus expected that the PPh_3 group of the $[\text{Rh}(\text{fctfa})(\text{CH}_3)(\text{CO})(\text{PPh}_3)(\text{I})\text{-alkyl}1]$ isomers in Scheme 1 should be positioned in the square plane

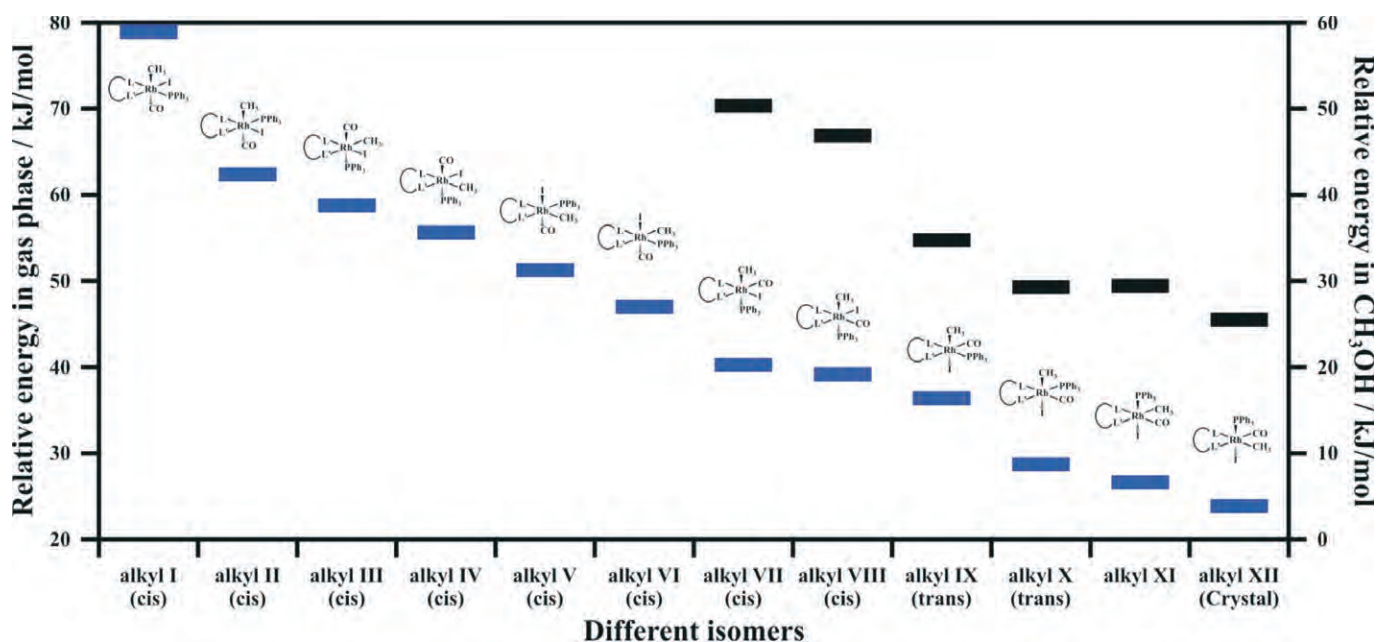


Figure 11 PW91/TZP calculated relative energies (kJ/mol) of the different isomeric forms of octahedral $[\text{Rh}(\text{fctfa})(\text{CH}_3)(\text{CO})(\text{PPh}_3)(\text{I})]$ -alkyl complexes in gas phase (blue) and in CH_3OH solution (black). The structure of alkyl XII corresponds to alkyl2, characterized by X-ray crystal structure.⁷⁸

formed by the β -diketonato ligand and the other two groups bonded to the rhodium centre of which the methine proton singlets are at 6.10 ppm (alkyl I isomers overlap), see reference 24 for a full discussion on NMR spectroscopy and computational chemistry results of the $[\text{Rh}(\text{fctfa})(\text{CO})(\text{PPh}_3)] + \text{CH}_3\text{I}$ reaction).

Finally DFT calculations were done to establish the relative stability of the different $[\text{Rh}(\text{fctfa})(\text{CH}_3)(\text{CO})(\text{PPh}_3)(\text{I})]$ -alkyl reaction products. PW91/TZP calculated relative molecular energies of 12 possible octahedral Rh^{III} -alkyl reaction products of $[\text{Rh}(\text{fctfa})(\text{CO})(\text{PPh}_3)]$ with CH_3I for gas phase calculations, as well as in methanol solution are illustrated in Fig. 11. When comparing the relative energies of the different Rh^{III} -alkyl complexes in Fig. 11, the lowest energy alkyl isomers are alkyls XI and XII. Stereo arrangement of the calculated most stable alkyl XII corresponds to the isolated $[\text{Rh}(\text{fctfa})(\text{CH}_3)(\text{CO})(\text{PPh}_3)(\text{I})]$ -alkyl2 reaction product characterized by X-ray crystallography, in Scheme 1.

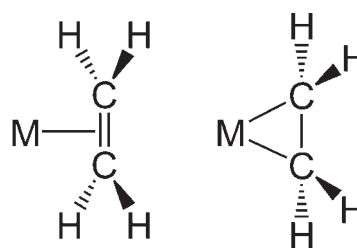
3.6. Bonding and Structure⁹¹

Transition-metal-ethylene complexes are among the most important classes of compounds in chemistry. For example, the first organometallic compound to be isolated in pure form, is the Zeise's platinum-ethylene complex, $\text{K}[\text{PtCl}_3(\text{C}_2\text{H}_4)] \cdot \text{H}_2\text{O}$ (Zeise's salt, synthesized in 1827).^{92–94} Complexes of coinage metals (Cu, Ag and Au) and alkenes have significant application in organic synthesis^{95–97} and in several industrial catalytic processes.⁹⁸ The Dewar-Chat-Duncanson model^{99,100} describes the bonding in coinage-metal-ethylene complexes as a synergistic combination of σ -donor and π -acceptor interactions between the metal ion and the ethylene π -system. The bonding between metal-ethylene complexes can vary from a T-shaped structure to a metallacyclopropane, see Scheme 2. In the T-shaped structure, the ethylene-metal-ion interaction is weak and typically dominated by the ethylene-to-metal-ion σ -donation (leading to the T-shaped structure). At the other extreme, σ -donation and, more importantly, the metal-ion-to-ethylene π -back-donation is dominant, and it results in a metallacyclopropane ring structure and a $\text{C}=\text{C}$ bond with a bond order approaching unity.¹⁰¹ Since both the σ -donor and π -back-bonding contributions lead to the lengthen-

ing of the $\text{C}=\text{C}$ bond, metal-ethylene adducts should show $\text{C}=\text{C}$ distances that are longer than that of free ethylene.¹⁰¹

The CC bond distance has been extensively evaluated as a measure of metal/olefin interaction. Within the Dewar-Chat-Duncanson (DCD) model,^{99,100} both ligand-to-metal σ -donation from π_{CC} and metal-to-ligand π -backbonding to the π^*_{CC} orbital will lengthen the ethylene CC bond, which is expected to range from 1.34 Å (π -complex, T-shaped structure) to 1.54 Å (metallacyclopropane). Ethylene complexes of copper,¹⁰² silver¹⁰³ and gold¹⁰⁴ supported by tris(pyrazolyl)borates (Tp) provide an interesting example of the κ^3 to κ^2 coordination of the Tp ligand. Crystal structures of $[\text{HB}(3,5\text{-}(\text{CF}_3)_2\text{Pz}_3)_3\text{M}(\text{C}_2\text{H}_4)]$ with the fluorinated hydrotris(pyrazolyl)borate supporting ligand, display κ^3 coordination for $\text{M} = \text{Cu}$ and Ag , but κ^2 coordination of the tris(pyrazolyl)borate ligand (i.e., one very long and two short Au-N bond lengths) for the Au complex, see Fig. 12.

Data from computational and experimental sources (especially ¹³C chemical shifts) have been combined to address the bonding and structure of $[\text{RB}(3\text{-}(\text{R}^1),5\text{-}(\text{R}^2)\text{Pz})_3]\text{M}(\text{C}_2\text{H}_4)$ complexes, where $\text{M} = \text{Cu}, \text{Ag}, \text{Au}$ and $\text{R} = \text{H}$ or CH_3 .⁹¹ DFT (BP86 functional) optimized geometries of a series of $[\text{RB}(3\text{-}(\text{R}^1),5\text{-}(\text{R}^2)\text{Pz})_3]\text{M}(\text{C}_2\text{H}_4)$ complexes ($\text{M} = \text{Cu}, \text{Ag}, \text{Au}$) have an average calculated CC distance of 1.389(4), 1.380(4) and 1.422(6) Å for $\text{M} = \text{Cu}, \text{Ag}$ and Au , respectively. The CC bond length of free ethylene at this level of theory is 1.338 Å, i.e. $\sim 4\%$ lengthening of the CC bond upon coordination to copper. The average CC distance of the $[\text{RB}(3\text{-}(\text{R}^1),5\text{-}(\text{R}^2)\text{Pz})_3]\text{Au}(\text{C}_2\text{H}_4)$ complexes are thus significantly



Scheme 2

Limiting structures of a metal-ethylene complex: T-shaped structure (left) and metallacyclopropane (right).

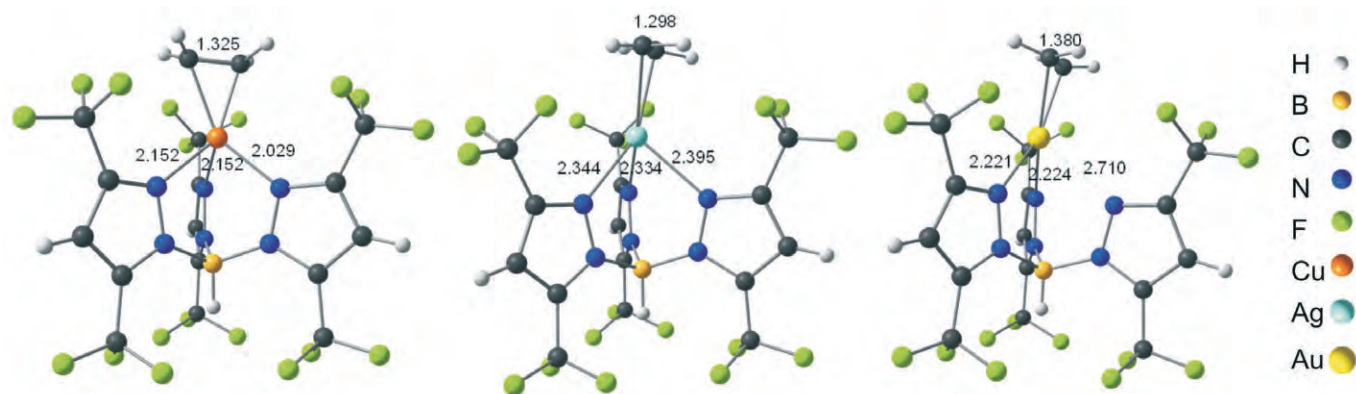


Figure 12 A presentation of the crystal structures of $[\text{HB}(3,5\text{-(CF}_3)_2\text{Pz)}_3]\text{M}(\text{C}_2\text{H}_4)$ for $\text{M} = \text{Cu}$ (left) Ag (middle) and Au (right).

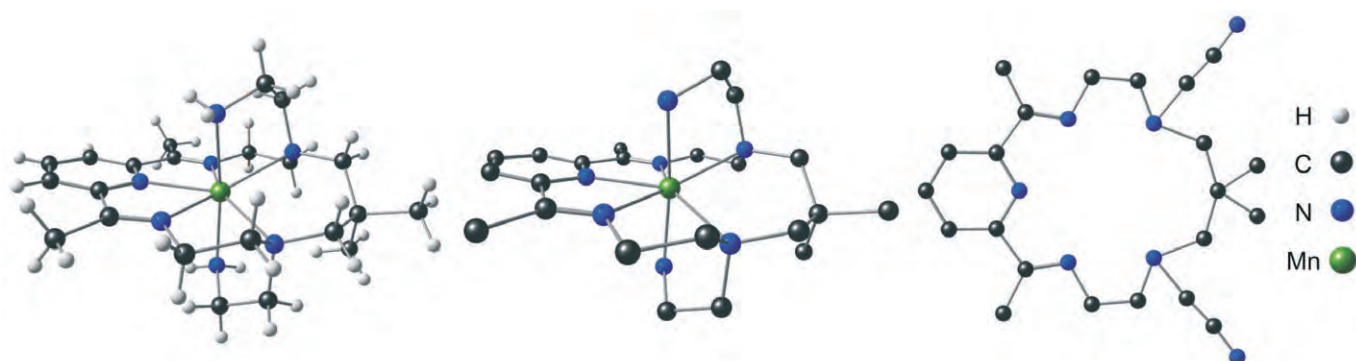


Figure 13 The experimental geometry of $[\text{MnL}^7]^{2+}$ (left), with hydrogen atoms removed for clarity (middle) and a flat presentation of the L^7 ligand (right).

shorter than the Ag and Cu congeners. In evaluating the κ^3 to κ^2 distortion of the $[\text{RB}(3\text{-(R}^1)\text{,5-(R}^2)\text{Pz)}_3]\text{M}(\text{C}_2\text{H}_4)$ complexes ($\text{M} = \text{Cu, Ag, Au}$), the asymmetry within the studied scorpionate complexes is defined as $Asym = \text{stdev}(\text{MN})/\text{average}(\text{MN}) \times 100\%$. Calculated $Asym$ values were found to be the largest for Au (14(2)%), Cu intermediate (8(1)%), and least for Ag (6(1)%), all in agreement with experimental structures, see Fig. 12.

NMR analysis of bonding in transition metal olefin complexes proved to be a valuable tool, e.g. Cundari *et al.* focused on experimental and calculated ^{13}C chemical shifts.⁹¹ Calculated free ethylene ^{13}C chemical shifts of 128.5 ppm compare well with experimental values of 123.4 ppm in CD_2Cl_2 . Calculated $\delta(^{13}\text{C})$ for the series of $[\text{RB}(3\text{-(R}^1)\text{,5-(R}^2)\text{Pz)}_3]\text{M}(\text{C}_2\text{H}_4)$ complexes ($\text{M} = \text{Cu, Ag, Au}$) were in accord with experimental chemical shifts that have been reported. Calculated chemical shifts are closest to free ethylene for the silver complexes. The gold complexes, on the other hand, display the lowest chemical shifts (or most upfield shifted ^{13}C signals relative to free ethylene) among the coinage metal systems studied.⁹¹ To further calibrate the coinage metal complexes studied, a literature survey of ^{13}C NMR chemical shifts was conducted. The survey yielded ^{13}C NMR chemical shifts for 30 complexes with a median of 60 ppm, a sample mean and standard deviation of 57 ± 18 ppm. ^{13}C NMR chemical shifts ranged from 25 ppm (for $[\text{Ni}(\text{Pr}_2\text{Im})_2(\text{C}_2\text{H}_4)]$ considered as the most metallacyclopropane) to 105 ppm (for $[\text{HB}(3,5\text{-(CF}_3)_2\text{Pz)}_3]\text{Ag}(\text{C}_2\text{H}_4)$), the 'most π -complex' in bonding character.⁹¹ Gold complexes are the least π -complex/most metallacyclopropane in their nature, and vice versa for the silver congeners. Hence, NMR results and calculations support (and extend) structural analyses.

3.7. Symmetry and Structure¹⁰⁵

The last example is a series of metal(II) complexes coordinated to a 16-membered pentaaza macrocycle having two 2-aminoethyl pendant arms [2,14-dimethyl-6,10-bis(2-aminoethyl)-3,6,10,13,19-pentaazabicyclo[13.3.1]8,8-dimethylnonadecane-1(19),2,13,15,17-pentaene] (abbreviated as L^7 , $\text{M} = \text{Mg, Mn, Zn}$ and Cd). The geometry of the coordination sphere of $[\text{MnL}^7]^{2+}$ and $[\text{MgL}^7]^{2+}$ is determined from X-ray crystallography as a slightly distorted pentagonal bipyramid with the metal ion located within a pentaaza macrocycle and two pendant amines coordinating on opposite sides, see Fig. 13.

^{13}C and ^1H NMR spectra of the complexes with $\text{M} = \text{Mg, Zn}$ and Cd show C_2 symmetry, which is in agreement with a heptadentate pentagonal bipyramidal geometry in solution. HF and DFT calculations predicted structures with C_2 symmetry, which is closely approximated in the solid state structures of $[\text{MgL}^7]^{2+}$ and $[\text{MnL}^7]^{2+}$.

Acknowledgements

Financial assistance by the Central Research Fund of the University of the Free State and the National Research Foundation of South Africa is gratefully acknowledged.

References and Notes

- 1 M. Avalos, R. Babiano, M.J. Carretero, P. Cintas, F.J. Higes, J.L. Jimenez and J.C. Palacios, *Tetrahedron*, 1998, 54, 615.
- 2 A. Vulpetti, N. Schiering and C. Dalvit, *Proteins*, 2010, 3281.
- 3 N. Goudreau, D.R. Cameron, R. Deziel, B. Hache, A. Jakalian, E. Malenfant, J. Naud, W.W. Ogilvie, J. O'Meara, P.W. White and C. Yoakima, *Bioorganic & Medicinal Chemistry*, 2007, 15, 2690.
- 4 R. Annunziata, L. Raimondi, G.M. Nano, G. Palmisano and S.

- Tagliapietra, *Magnetic Resonance in Chemistry*, 1997, **35**, 721.
- 5 The calculation of NMR parameters of transition metal complexes using DFT methods is reviewed in J. Autschbach, *Structure and Bonding*, 2004, **112**, 1–43.
- 6 W.J. Hehre, *A Guide to Molecular Mechanics and Quantum Chemical Calculations*; 2003, Wavefunction, Inc., Irvine, CA, 1998. See also the compilations therein.
- 7 W.J. Hehre and L. Lou, *A Guide to Density Functional Calculations in Spartan*; Wavefunction, Inc.: Irvine, CA, 1997.
- 8 J.B. Foresman and A. Frisch, *Exploring Chemistry with Electronic Structure Methods*; Gaussian, Inc., Pittsburgh, 1996.
- 9 F. Jensen, *Introduction to Computational Chemistry*; Wiley: New York, 1999.
- 10 A.D. Becke, *Phys. Rev.* 1988, **A38**, 3098.
- 11 A.D. Becke, *J. Chem. Phys.* 1997, **107**, 8554.
- 12 J.D. Perdew, Y. Wang, *Phys. Rev. B* 1986, **33**, 8800 (b) J.P. Perdew, *Phys. Rev. B* 1986, **33**, 5048, 8822. (c) J.P. Perdew, *Phys. Rev. B* 1986, **34**, 7406.
- 13 J.P. Perdew, S.H. Chevary, K.A. Vosko, M.R. Jackson, M.R. Pederson, D.J. Singh and C. Fiolhais, *Phys. Rev. B* 1992, **46**, 6671–6687. Erratum: J.P. Perdew, J.A. Chevary, S.H. Vosko, K.A. Jackson, M.R. Pederson, D.J. Singh and C. Fiolhais, *Phys. Rev. B*, 1993, **48**, 4978.
- 14 A.D. Becke, *J. Chem. Phys.* 1996, **104**, 1040.
- 15 C. Lee, W. Yang and R.G. Parr, *Phys. Rev.* 1988, **B41**, 785–789.
- 16 (a) A.D. Becke, *J. Chem. Phys.* 1993, **98**, 5648. (b) A.D. Becke, *J. Chem. Phys.* 1992, **96**, 2155. (c) A.D. Becke, *J. Chem. Phys.* 1992, **97**, 9173.
- 17 The OPTX exchange functional: N.C. Handy, A. Cohen, *J. Mol. Phys.* 2001, **99**, 403–418.
- 18 The DFT calculations were carried out with the ADF2007 program system using methods described in: G.T. Velde, F.M. Bickelhaupt, E.J. Baerends, C.F. Guerra, S.J.A. Van Gisbergen, J.G. Snijders and T. Ziegler, *J. Comput. Chem.* 2001, **22**, 931–967.
- 19 All case studies were previously published by the author and other groups. The discussion in this review is different from work published previously with the main focus on DFT and NMR.
- 20 A. Kuhn, T.A. Tsoetsi and J. Conradie, *Inorg. Chim. Acta.*, 2009, **362**, 3088–3096.
- 21 A.J. Muller and J. Conradie, W. Purcell, S.S. Basson and J. A. Venter, *S. Afr. J. Chem.*, 2010, **63**, 11–19.
- 22 M.M. Conradie and J. Conradie, *J. Organomet. Chem.*, 2010, **695**, 2126–2133.
- 23 M.M. Conradie and J. Conradie, *Dalton Trans.*, 2011, **40**, 8226–8237.
- 24 M.M. Conradie and J. Conradie, *S. Afr. J. Chem.*, 2008, **61**, 102–111.
- 25 Y. Qian, J. Huang, M.D. Bala, B. Lian, H. Zhang and H. Zhang, *Chem. Rev.*, 2003, **103**, 2633–2690.
- 26 R. Beckhause and C. Santamaria, *J. Organomet. Chem.*, 2001, **617-618**, 81–97.
- 27 E. Manek, D. Hinz and G. Meyer, *Coord. Chem. Rev.*, 1997, **164**, 5–25.
- 28 J.C. Vites and M.M. Lynam, *Coord. Chem. Rev.*, 1995, **146**, 1–15.
- 29 J.C. Vites and M.M. Lynam, *Coord. Chem. Rev.*, 1995, **138**, 71–86.
- 30 R.O. Duthaler and A. Hafner, *Chem. Rev.*, 1991, **92**, 807–832.
- 31 E. Melendez, *Crit. Rev. Oncol. Hematol.*, 2002, **42**, 309–315.
- 32 B.K. Keppler, C. Friesen, H.G. Moritz and H. Vongerichten, E. Vogel, *Struct. Bonding*, 1991, **78**, 97–127.
- 33 P. Köpf-Maier, *Eur. J. Clin. Pharmacol.*, 1944, **47**, 1–16.
- 34 E. Dubler, R. Buschmann and H.W. Schmalle, *J. Inorg. Biochem.*, 2003, **95**, 97–104.
- 35 T.A. Tsoetsi, A. Kuhn, A. Muller and J. Conradie, *Polyhedron*, 2009, **28**, 209–214.
- 36 Cambridge Structural Database (CSD), Version 5.32, May 2011 update.
- 37 N. Yoneda, S. Kusano, M. Yasui, P. Pujado and S. Wilcher, (2001). *Appl. Catal. A: Gen.*, **221**, 253–265.
- 38 J.H. Jones, *Platinum Metal Review*, 2000, **44**, 94–105.
- 39 G.J. Sunley and D.J. Watson, *Catalysis Today*, 2000, **58**, 293–307.
- 40 A. Haynes, P.M. Maitlis, G.E. Morris, G.J. Sunley, H. Adams, P.W. Badger, C.M. Bowers, B. Cook, P.I.P. Elliot, T. Ghaffar, H. Green, T.R. Griffin, M. Payne, J.M. Pearson, M.J. Taylor, P.W. Vickers and R. J. Watt, *J. Am. Chem. Soc.*, 2004, **126**, 2847–2861.
- 41 T.W. Dekleva and D. Foster, *Adv. Catal.*, 1986, **34**, 81–130.
- 42 P.M. Maitlis, A. Hayes, G.J. Sunley and M.J. Howard, *J. Chem. Soc., Dalton Trans.*, 1996, 2187–2196.
- 43 A. Hayes, B.E. Mann, D.J. Gulliver, G.E. Morris and P.M. Maitlis, *Am. Chem. Soc.*, 1991, **113**, 8567–8569.
- 44 S.S. Basson, J.G. Leipoldt, A. Roodt and J.A. Venter, *Inorg. Chim. Acta*, 1987, **128**, 31–37.
- 45 J.G. Leipoldt, S.S. Basson and L.J. Botha, *Inorg. Chim. Acta*, 1990, **168**, 215–220.
- 46 J.G. Leipoldt, G.J. Lamprecht and G.J. van Zyl, *Inorg. Chim. Acta*, 1985, **96**, L31–L34.
- 47 M. Theron, E. Grobbelaar, W. Purcell and S.S. Basson, *Inorg. Chim. Acta*, 2005, **358**, 2457–2463.
- 48 E. Grobbelaar, W. Purcell and S.S. Basson, *Inorg. Chim. Acta*, 2006, **359**, 3800–3860.
- 49 J. Rankin, A.D. Poole, A.C. Benyei and D.J. Cole-Hamilton, *Chem. Comm.*, 1997, 1835–1836.
- 50 C.M. Thomas, A. Neels, H. Stoekli-Evans and G. Süß-Fink, *Eur. J. Inorg. Chem.*, 2001, 3005–3008
- 51 J.A. Gaunt, V.C. Hayens, S.K. Spitzmesser, A.J.P. White and D.J. Williams, *Organometallics*, 2004, **23**, 1015–1023.
- 52 H.M. Burke, J.F. Gallagher, M.T. Indelli and J.G. Vos, *Inorg. Chim. Acta*, 2004, **357**, 2989–3000.
- 53 M.P. Garcia, J.A. Manero, L.A. Oro, M.C. Aperda, F.H. Cano, J.G. Haasnoot, R. Prins and J. Reedijk, *Inorg. Chim. Acta*, 1986, **122**, 235–241.
- 54 L. Cavallo, M. Sola, *J. Am. Chem. Soc.*, 2001, **123**, 12294–12302.
- 55 J. Rankin, A.C. Benyei, A.D. Poole and D.J. Cole-Hamilton, *J. Chem. Soc., Dalton Trans.*, 1999, 3771–3782.
- 56 D. Forster, *Adv. Organomet. Chem.*, 1979, **17**, 255–267.
- 57 A. Haynes, B.E. Mann, G.E. Morris and P.M. Maitlis, *J. Am. Chem. Soc.*, 1993, **115**, 4093–4100.
- 58 T.R. Griffin, D.B. Cook, A. Haynes, J.M. Pearson, D. Monti and G.E. Morris, *J. Am. Chem. Soc.*, 1996, **118**, 3029–3030.
- 59 M. Cheong, R. Schmid and T. Ziegler, *Organometallics*, 2000, **19**, 1973–1982.
- 60 T. Kinnunen and K. Laasonen, *J. Mol. Struct. (Theochem)*, 2001, **542**, 273–288.
- 61 M. Cheong and T. Ziegler, *Organometallics*, 2005, **24**, 3053–3058.
- 62 V. Chauby, J.-C. Daran, C.S.-L. Berre, F. Malbosc, P. Kalck, O.D. Gonzalez, C.E. Haslam and A. Haynes, *Inorg. Chem.*, 2002, **41**, 3280–3290.
- 63 J.A. Venter, J.G. Leipoldt and R. van Eldik, *Inorg. Chem.*, 1991, **30**, 2207–2209.
- 64 M.R. Galding, T.G. Cherkasova, L.V. Osetrova, Y.S. Varshavsky and A. Roodt, *Rhodium Express*, 1996, **16**, 23–36.
- 65 A. Roodt, J.M. Botha, S. Otto, E.P. Shestakova and Y.S. Varshavsky, *Rhodium Express*, 1996, **17**, 4–9.
- 66 M.M. Conradie J.J.C. Erasmus and J. Conradie, *Polyhedron.*, 2011, **30**, 2345–2353.
- 67 J.G. Leipoldt, E.C. Steynberg and R. van Eldik, *Inorg. Chem.*, 1987, 3068–3070.
- 68 G.J. van Zyl, G.J. Lamprecht, J.G. Leipoldt and T.W. Swaddle, *Inorg. Chim. Acta*, 1988, **143**, 223–227.
- 69 G.J. van Zyl, G.J. Lamprecht and J.G. Leipoldt, *Inorg. Chim. Acta*, 1987, **129**, 35–37.
- 70 G.J. Lamprecht, G.J. Van Zyl and J.G. Leipoldt, *Inorg. Chim. Acta*, 1989, **164**, 69–72.
- 71 G.J. Van Zyl, G.J. Lamprecht and J.G. Leipoldt, *Inorg. Chim. Acta*, 1986, **122**, 75–79.
- 72 M. Feliz, Z. Freixa and P.W.N.M. van Leeuwen, C. Bo, *Organometallics*, 2005, **24**, 5718–5723.
- 73 S.S. Basson, J.G. Leipoldt and J.T. Nel, *Inorg. Chim. Acta*, 1984, **84**, 167–172.
- 74 S.S. Basson, J.G. Leipoldt, A. Roodt, J.A. Venter and T.J. van der Walt, *Inorg. Chim. Acta*, 1986, **119**, 35–38.
- 75 Y.S. Varshavsky, T.G. Cherkosova, N.A. Buzina and L. S. Bresler, *J. Organomet. Chem.*, 1994, **464**, 239–245.
- 76 A. Brink, A. Roodt, G. Steyl and H. G. Visser, *Dalton Trans.*, 2010, **39**, 5572–5578.
- 77 J. Conradie and J.C. Swarts, *Organometallics* 2009, **28**, 1018–1026.

- 78 J. Conradie, G.J. Lamprecht, A. Roodt and J.C. Swarts, *Polyhedron*, 2007, **23**, 5075–5087.
- 79 M.M. Conradie and J. Conradie, *Inorg. Chim. Acta*, 2008, **361**, 2285–2295.
- 80 N.F. Stuurman and J. Conradie, *J. Organomet. Chem.*, 2009, **694**, 259–268.
- 81 M.M. Conradie and J. Conradie, *Inorg. Chim. Acta*, 2008, **361**, 208–218.
- 82 A.W. Overhauser, *Phys. Rev.*, 1953, **92**, 411–415.
- 83 T.R. Carver and C. P. Slichter, *Phys. Rev.*, 1953, **92**, 212–213.
- 84 C.P. Slichter, *Principles of Magnetic Resonance*, 3rd edn., Springer, Berlin and New York, 1996.
- 85 L.J. Damoense, W. Purcell, A. Roodt and J.G. Leipoldt, *Rhodium Ex.*, 1994, **5**, 10–13.
- 86 K.G. van Aswegen, J.G. Leipoldt, I.M. Potgieter, G.J. Lamprecht, A. Roodt and G.J. van Zyl, *Transition Met. Chem.*, 1991, **16**, 369–371.
- 87 P. Braunstein, Y. Chauvin, J. Fischer, H. Olivier, C. Strohmman and D.V. Toronto, *New J. Chem. (Nouv. J. Chim.)*, 2000, **24**, 437–445.
- 88 S.S. Basson, J.G. Leipoldt, A. Roodt and J.A. Venter, *Inorg. Chim. Acta*, 1987, **128**, 31–37.
- 89 G.J. Lamprecht, J.C. Swarts, J. Conradie and J.G. Leipoldt, *Acta Cryst.*, 1993, **C49**, 82–84.
- 90 J. Clayden, N. Greeves, S. Warren and P. Wothers, *Organic Chemistry*, Oxford University Press, 2001, 251.
- 91 A.B. Kazi, H.V.R. Dias, S.M. Tekarli, G.R. Morello and T.R. Cundari, *Organometallics*, 2009, **28**, 1826–1831.
- 92 L.B. Hunt, *Platinum Met. Rev.* 1984, **28**, 76–83.
- 93 C. Elschenbroich, *Organometallics*, 3rd edn, VCH, Weinheim, 2006.
- 94 R.N. Keller, *Chem. Rev.* 1941, **28**, 229–267.
- 95 H. Schmidbaur, A. Schier, 'Gold Organometallics' in *Comprehensive Organometallic Chemistry III*, vol. 2, Elsevier, Amsterdam, 2007.
- 96 P.J. Perez, M.M. Diaz-Requejo, Copper organometallics in *Comprehensive Organometallic Chemistry III*, vol. 2, Elsevier, Amsterdam, 2007.
- 97 A. Fuerstner, P.W. Davies, *Angew. Chem. Int. Ed.* 2007, **46**, 3410–3449.
- 98 K. Weissmehl, H.J. Arpe, *Industrial Organic Chemistry*, 3rd edn, VCH, Weinheim, 1997.
- 99 J. Chatt and L.A. Duncanson, *J. Chem. Soc.* 1953, 2939–2947.
- 100 M.J.S. Dewar, *Bull. Soc. Chim. Fr.* 1951, C71.
- 101 H.V.R. Dias and W. Jin, *Eur. J. Inorg. Chem.* 2008, **4**, 509–522.
- 102 H.V.R. Dias, H.L. Lu, H.J. Kim, A.A. Polach, T.K.H.H. Goh, R.G. Browning and C.J. Lovely, *Organometallics* 2002, **21**, 1466.
- 103 H.V.R. Dias; Z. Wang and W. Jin, *Inorg. Chem.* 1997, **36**, 6205.
- 104 H.V.R. Dias and J. Wu, *Angew. Chem., Int. Ed.* 2007, **46**, 7814.
- 105 H. Khanmohammad, S. Amani, H. Lang and T. Rueffe, *Inorg. Chim. Acta*, 2007, **360**, 579–587.